Structure
Article

Structure of the *Mtb* CarD/RNAP β-Lobes Complex Reveals the Molecular Basis of Interaction and Presents a Distinct DNA-Binding Domain for *Mtb* CarD

Gulcin Gulten[1] and James C. Sacchettini[1,2,*]
[1]Department of Chemistry
[2]Department of Biochemistry and Biophysics
Texas A&M University, College Station, TX 77843, USA
*Correspondence: sacchett@tamu.edu
http://dx.doi.org/10.1016/j.str.2013.08.014

SUMMARY

CarD from *Mycobacterium tuberculosis* (*Mtb*) is an essential protein shown to be involved in stringent response through downregulation of rRNA and ribosomal protein genes. CarD interacts with the β-subunit of RNAP and this interaction is vital for *Mtb*'s survival during the persistent infection state. We have determined the crystal structure of CarD in complex with the RNAP β-subunit β1 and β2 domains at 2.1 Å resolution. The structure reveals the molecular basis of CarD/RNAP interaction, providing a basis to further our understanding of RNAP regulation by CarD. The structural fold of the CarD N-terminal domain is conserved in RNAP interacting proteins such as TRCF-RID and CdnL, and displays similar interactions to the predicted homology model based on the TRCF/RNAP β1 structure. Interestingly, the structure of the C-terminal domain, which is required for complete CarD function in vivo, represents a distinct DNA-binding fold.

INTRODUCTION

Tuberculosis (TB) is a global health threat responsible for approximately two million deaths annually (http://www.who.int/tb). The treatment for the primary causative agent of TB, *Mycobacterium tuberculosis* (*Mtb*), is challenging due to the emergence of multidrug (MDR-TB) and extensively drug-resistant (XDR-TB) strains. Because most of the antibiotics currently used for *Mtb* therapy are potent only against replicating bacteria, mycobacteria are able to survive in the host in a nonreplicating, persistent, or chronic state. Identifying new drugs that can target *Mtb* during the persistent stages of infection is very important (Gupta et al., 2009; Raman et al., 2008; Sacchettini et al., 2008).

In *Mtb*, the gene product of *Rv3583c*, annotated CarD, is required for persistence, and has been identified as an essential protein in vitro and in vivo during normal growth conditions as well as under genotoxic stress and nutrient deprivation (Stallings et al., 2009). Microarray studies have shown that not only is *Rv3583c* upregulated in response to oxidative stress, DNA damage, and starvation, but also that depletion of *Mtb* CarD results in loss of transcriptional regulation of rRNA and ribosomal components, indicating its involvement in stringent response (Stallings et al., 2009). *Mtb* CarD can be used to complement *Escherichia coli* DksA protein, which regulates stringent response alongside the main stringent response element hyperphosphorylated guanine nucleotide ((p)ppGpp), suggesting that the two proteins are functional homologs. DksA directly interacts with the RNA polymerase (RNAP) through the RNAP secondary channel and potentiates the effect of (p)ppGpp (Paul et al., 2004b; Srivatsan and Wang, 2008). *Mtb* produces (p)ppGpp, but does not have a DksA homolog.

The first and best studied CarD protein is from *Myxococcus xanthus* and is a transcription regulator involved in carotenogenesis. *M. xanthus* CarD interacts with RNAP, CarG, and the *carQRS* promoter DNA through its N- and C-terminal domains (Nicolas et al., 1996; Peñalver-Mellado et al., 2006). *Mtb* CarD shares only a 30% sequence homology with the N terminus of *M. xanthus* CarD, and the C-terminal domain is not similar, suggesting that *Mtb* CarD does not contain the HMG1-like DNA-binding domain (AT hook DNA-binding motif sequence) found in *M. xanthus* CarD (Figure S1 available online). Bacterial two hybrid assays and immunoprecipitation experiments have shown that *Mtb* CarD associates with the RNAP β-subunit (Stallings et al., 2009; Weiss et al., 2012). All CarD and CarD N-terminal like (CdnL) proteins belong to the transcription-repair coupling factor (TRCF) family of proteins, and share sequence and structural homology with the TRCF RNAP interacting domain (RID). Also, they are thought to interact with RNAP in a homologous manner as TRCF. The previously determined crystal structure of the *Tth* TRCF-RID/*Taq* RNAP β1 complex (Westblade et al., 2010) and the homology models generated for CarD-RNAP interaction based on this structure (Weiss et al., 2012) predicted a similar set of interactions of CarD with RNAP. However, the mechanism CarD uses to regulate RNAP function and transcription, and the role of the *Mtb* CarD C-terminal domain are unknown. The CarD/RNAP interaction is crucial for *Mtb*'s stringent response, viability, and resistance to oxidative stress and loss of the CarD/RNAP interaction sensitizes *Mtb* to the anti-TB drug rifampicin, emphasizing the importance of understanding this protein-protein interaction.

Here, we report the crystal structure of *Mtb* CarD complexed with the *Mtb* RNAP β-subunit lobe domains at 2.1 Å resolution. The CarD/RNAP β structure reveals that the RNAP CarD binding

Table 1. Data Collection and Refinement Statistics

	Se-Met RpoBtr	Native RpoBtr	CarD/RpoBtr complex
Data Collection			
Space group	$P2_12_12_1$	$P2_12_12_1$	$C222_1$
Cell Dimensions			
a, b, c (Å)	52.8, 124.1, 135.5	53.1, 123.9, 135.6	49.1, 128.9, 225.5
α, β, γ (°)	90, 90, 90	90, 90, 90	90, 90, 90
Wavelength (Å)	0.979	0.979	0.979
Resolution (Å)	2.8 (2.79)	2.5 (2.45)	2.1 (2.11)
Completeness (%)	98.5 (90.3)	99.5 (97)	98.1 (92)
Redundancy	3.1 (3.1)	7.0 (6.3)	4.8 (4.6)
I/Iσ	13.9 (2.4)	15.1 (1.9)	10.1 (2.0)
R_{sym} (%)	5.28 (53.4)	5.45 (65.7)	7.8 (73.14)
Refinement			
Resolution	48.6–2.79	49–2.45	37.6–2.11
No. reflections	22,552	33,551	40,747
R_{work}/ R_{free}	0.24/0.28	0.21/0.26	0.20/0.23
No. of Atoms			
Protein	5,844	6,097	4,203
Water	19	126	305
B-Factors			
Protein	95.2	46.4	31.4
Water	57.1	47.3	45.0
Rmsd			
Bond lengths (Å)	0.010	0.003	0.005
Bond angles (°)	1.52	0.68	0.87

Highest resolution shell values are given in parentheses.

site is located on the β-subunit arm of the RNAP claws, specifically on the solvent exposed surface of the β1 domain, and is far from the catalytic center of the RNAP. The structure not only provides insight into the molecular basis of RNAP interaction with *Mtb* CarD, but also with other CarD family proteins and CarD homologs. The structural basis for the RNAP regulation through CarD interaction, which is distinct from the DksA regulation mechanism, is presented by comparing the uncomplexed *Mtb* RNAP-β and CarD/RNAP-β complex structures. While the structural fold of the CarD N-terminal domain is conserved among other CarD, CdnL, and TRCF-RID domains, the C-terminal domain structure is not been identified in any other structure in the Protein Data Bank (PDB). We show that *Mtb* CarD is a DNA-binding protein with a distinct DNA-binding domain and that it exhibits a nonsequence-specific DNA-binding mode.

RESULTS AND DISCUSSION

Structure Determination of *Mtb* RpoBtr and the CarD/RNAP Complex

E. coli expression plasmids for the full-length *Mtb* RNAP β-subunit (RpoB) and several truncations (based on the secondary structure predictions) were made to test for recombinant protein expression. One truncation containing the β-lobes (consisting of residues 47–433) of RpoB (referred as RpoBtr) yielded soluble protein and when co-expressed with *Mtb* CarD resulted in complex formation, and it was chosen for subsequent crystallographic studies. The β1 (residues 47–172 and 375–428, corresponding to the *Taq*-β residues 1–130 and 334–395 of the TRCF/β1 structure) and β2 (residues 177–370) domains contained within this truncation are important for RNAP regulation. They form the β-arm of the RNAP claws that cover the DNA/RNA hybrid and dsDNA in the transcription complex. Regulation through these domains often occurs through interaction with various regulatory proteins such as TRCF and sigma70 (Vassylyev et al., 2002; Westblade et al., 2010). RpoB does not have any dispensable regions, and the archaebacterial split site, which maps around residue 570 of RpoB, is not contained within the β-subunit truncation used in this work. Crystals of RpoBtr were determined to be in the $P2_12_12_1$ space group with two molecules in the ASU. The RpoBtr structure was solved by single-wavelength anomalous diffraction using Se-Met derived crystals to a resolution of 2.9 Å. Subsequently, the resolution was improved to 2.5 Å for native (non Se-Met) RpoBtr crystals. The structure was refined to R_{work} = 21% and R_{free} = 26%, with excellent stereochemistry (Table 1).

Full-length CarD bound to RpoBtr was crystallized after co-expression and purification of the complex. The crystals belonged to the $C222_1$ space group with a single copy of the heterodimer in the ASU. The structure of the CarD/RpoBtr complex (hereafter referred to as the CarD/RNAP complex) was determined by molecular replacement, using the uncomplexed RpoBtr β1 and β2 domain structures as two individual search molecules. After locating RpoBtr using molecular replacement and initial refinement, there was clear electron density $|F_o|-|F_c|$ that was unaccounted for (Figure S2A). This extra electron density belonged to the protein, and the entire atomic model of CarD was manually built into the difference electron density map. The crystal structure of the complex was refined to R_{work} = 20% and R_{free} = 23% using diffraction data to 2.1 Å resolution.

Overall Structure of *Mtb* CarD

Mtb CarD belongs to the α + β protein class (SCOP) (Murzin et al., 1995). The structure is composed of two distinct domains: an all β-stranded N-terminal domain (residues 1–49) and an all α-helical C-terminal domain (residues 63–160; Figures 1A and 2A). The N- and C-terminal domains are connected by a six-residue twisted α helix (α1) and an eight residue loop. The N-terminal domain has a Tudor-like fold (Selenko et al., 2001) consisting of four antiparallel β strands. Residues Thr26, Ile27, Lys28, and Gly29, which lie on the β-turn connecting the β2 and β3 strands, were the only residues disordered in the N-terminal domain.

The structure of the CarD N-terminal domain is conserved among RNAP interacting proteins such as TRCF-RID and *Thermus thermophilus* (*Tth*) CdnL (CarD N-terminal like protein involved in cell division). Superposition of the *Mtb* CarD N-terminal domain structure with the *Tth* CdnL N-terminal domain (PDB ID: 2LQK; Gallego-García et al., 2012) and *Tth* TRCF-RID structures (PDB ID: 3MLQ; Westblade et al., 2010) gives a root-mean-square deviation (rmsd) of 1.1 Å over the C_α backbone for residues 1–49 (Figure 2A).

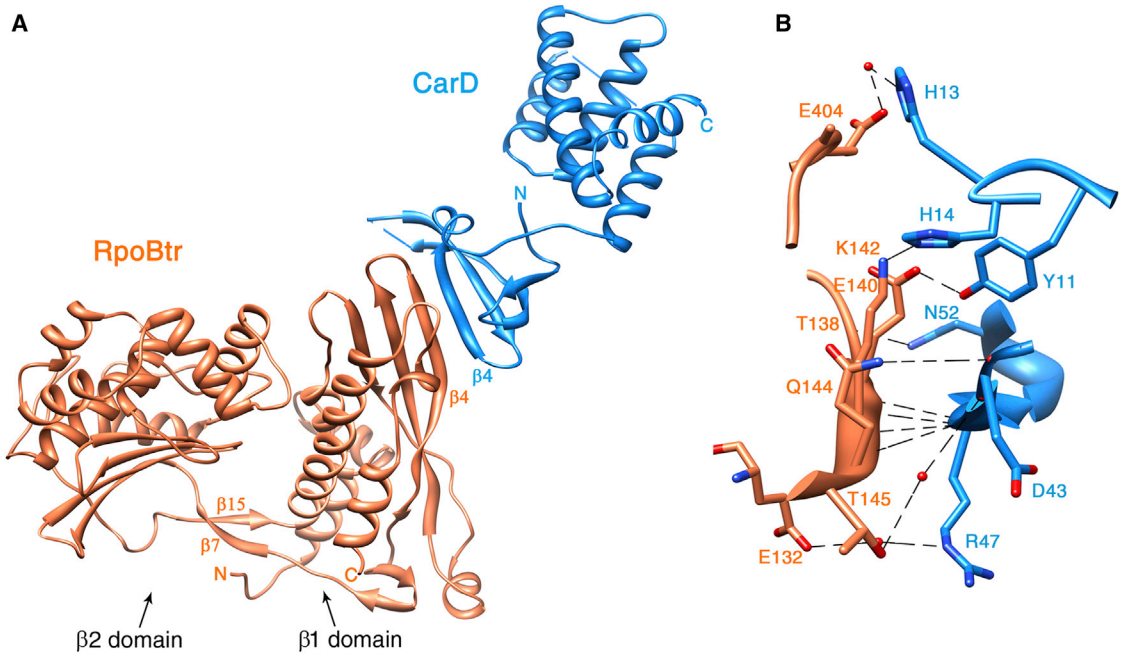

Figure 1. Ribbon Representation of the *Mtb* CarD/RNAP β1-β2 Domain Complex Structure

RpoBtr is represented by orange ribbons; CarD is represented by blue ribbons.

(A) Overall structure of the complex. β1 and β2 domains of RNAP β-subunit, β4 strands of each protein, and N and C termini of each chain are labeled. The interdomain bridging β sheet of RpoBtr (β7 and β15) is also indicated.

(B) Zoom of the CarD-RNAP interface. Direct and water-mediated H-bonding interactions between side chains and backbone-backbone interactions are shown. Hydrogen bonds and nonbonded contacts between RpoBtr and CarD are formed by the residues located on the β4 strands of both proteins, on the loop connecting α12 and α13 of the RNAP β1 domain, and on the turn between the β1 and β2 strands of CarD. H-bonds are represented by dashed lines and water molecules are shown in red spheres.

For the distances, refer to Table 2. See also Figure S2.

The CarD C-terminal domain is comprised of an α-helical bundle of five α helices that contains an unexpected internal leucine zipper between helices α4 and α5 (Figures 2B and 2C). Helices α4 and α5 interact only through hydrophobic and van der Waals interactions, afforded by the leucine zipper. Helices α2 and α3 are positioned parallel to each other, whereas α4, α5, and α6 pack orthogonally to each other. Helices α3 and α4 are connected by a γ-turn, while α4-α5 and α5-α6 are connected by β-turns (Figure 2B). The loop connecting α2 and α3, spanning residues His78 to Asn83, is completely disordered in the structure. The helices contain mostly hydrophobic amino acids at their helix-helix interfaces, generating a hydrophobic core. There are just two polar interactions inside this compact bundle, the hydrogen bonds between Lys95 (α3)-Glu106 (α4; 2.7 Å) and Arg132 (α5)-Asp155 (α6; 2.9 Å).

The three-helix bundle of α3, α4, and α5 is involved in DNA binding (see DNA-binding studies on *Mtb* CarD section for details). The structure of this three-helix bundle is unlike other DNA-binding proteins in the PDB, including all of the other HTH motifs and leucine zipper domains. DNA-binding proteins with classical HTH motifs usually insert their second (recognition) α helix in the major groove for base-specific DNA interaction. Leucine zippers containing DNA-binding proteins usually dimerize through the hydrophobic leucine zipper region, while also interacting with the major groove of the DNA; however, this is not the case for CarD. The DNA-interacting region of *Mtb* CarD is mapped to the N termini of α3 and α5, the C terminus of α4, and the β-turn connecting α4 and α5 (Figure 5). The leucine zipper motif of CarD appears to stabilize the conformation of α4 and α5 inside the hydrophobic core and is not involved directly in dimerization or DNA interaction (Figure 2C).

Neither the AT-hook DNA-binding motif of *M. xanthus* CarD nor any other recognizable DNA-binding motif is present in the *Mtb* CarD protein sequence. Structural similarity searches of the CarD C-terminal domain structure, using the PDBeFold, VAST, and DALI servers against the PDB and Structural Classification of Proteins database, did not identify any significant structural homologs. The structural alignment scores were well below the threshold of significance (VAST score < 5.5, VAST -log(p) value < 4.0, and Q-score < 0.49) for each alignment program (Gibrat et al., 1996; Holm and Rosenström, 2010; Krissinel and Henrick, 2004). It has been observed that the VAST hits do not share any common functional or structural features with *Mtb* CarD, besides being α-helical proteins.

Overall Structure of *Mtb* RNAP β1-β2 Domains

The RpoBtr structure reported here consists of the β1 and β2 domains of the *Mtb* RNAP β-subunit (corresponding to the protrusion and lobe domains, respectively, of eukaryotic RNAP II) that form the RNAP claws, together, with the β′ subunit. RNAP interacts with the transcription bubble nontemplate strand, especially with the G+2 base, through the β2 domain residues, and these

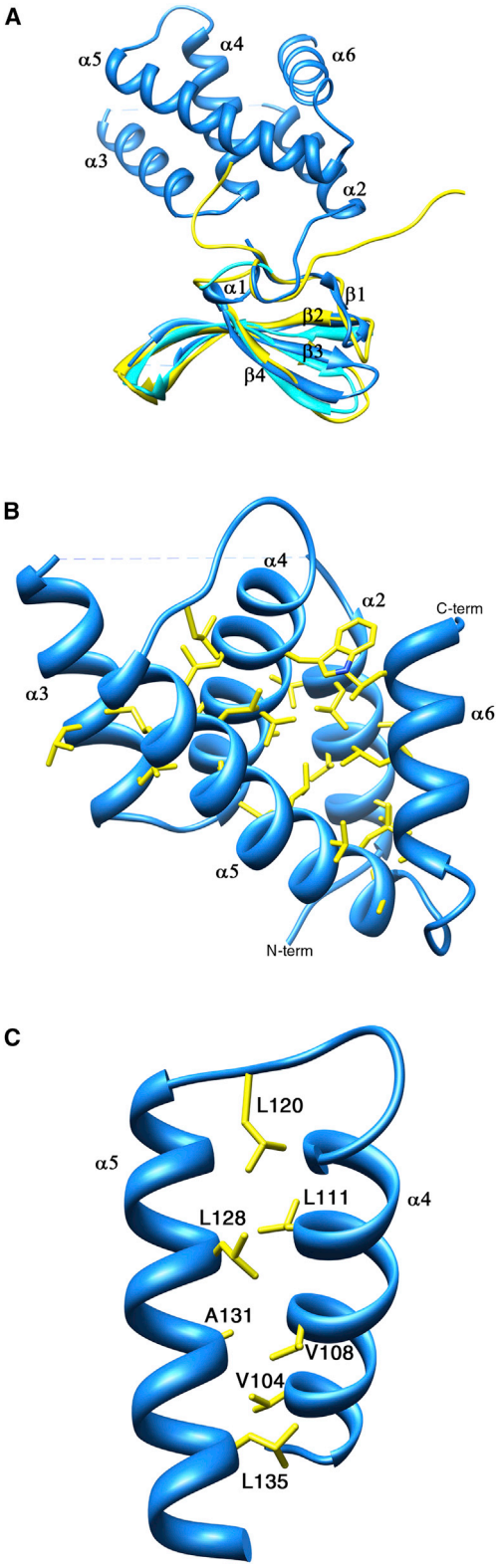

Figure 2. Ribbon Representation of *Mtb* CarD

(A) Superposition of *Mtb* CarD N-terminal domain structure (blue) with the *Tth* CdnL-NMR structure (yellow) and the *Tth* TRCF-RID structure (cyan). The RNAP-interacting β4 strand is labeled. The rmsd over the C_α backbone is 1.1 Å.

(B) Ribbon representation of the CarD C-terminal domain. The helices contain mostly hydrophobic amino acids at their helix-helix interfaces, generating a hydrophobic core. The remainder of the structure is omitted for clarity.

(C) The leucine zipper present between α4 and α5 in the C-terminal domain of CarD is formed by residues Leu120, Leu111, Leu128, and Leu135, and surrounded by hydrophobic residues Val104, Val108, and Ala131. The rest of the structure is omitted for clarity. The leucine zipper lies inside the hydrophobic core of CarD and is not involved in dimerization or DNA interaction. In both panels, hydrophobic residues are shown with yellow sticks.

See also Figure S1.

interactions are critical for sequence-specific promoter recognition of RNAP along with the transcription bubble formation and stability (Zhang et al., 2012).

The RpoBtr β1 domain aligns well with the β1 domain from the TRCF/β1 structure (rmsd 1.04 Å). However, superposition of the RpoBtr β1 domain with the *E. coli, Tth*, and *Taq* RNAP β-lobe structures gives an rmsd of approximately 10 Å over the C_α atoms of the β2 domain (Figures S3A and S3B). β-lobes are known to have conformational flexibility (Tagami et al., 2010), and the relative conformation adopted by the β1 and β2 domains of RpoBtr has not been observed in any other bacterial core or holo RNAP structure. The two molecules in the ASU of the uncomplexed RpoBtr structure, RpoBtr_A and RpoBtr_B, are also in different conformations. When the β1 domains of RpoBtr_A and RpoBtr_B are aligned, the rmsd of the C_αs of the β2 domains is 5.2 Å (over 191 atom pairs). The conformational difference observed in the β1-β2 domain-domain orientation can be explained by rotation around the hinge axis centered on the two stranded antiparallel β sheet connecting the two domains (Figure S3C).

The RNAP β-subunits are structurally highly conserved among different kingdoms, even though sequence conservation is low (Lane and Darst, 2010; Severinov et al., 1996). As expected, the secondary and the tertiary structure of the *Mtb* RNAP β1-β2 domains are almost identical to the *E. coli* and *Tth* RNAP β1-β2 domains (Figures S3A and S3B). The β1 domain (residues 47–172 and 375–428) consists of four antiparallel β strands flanked by five α helices on one side and one α-helix and a β-hairpin from the other side (Figure 3A). The β2 domain (residues 177–370) is composed of four antiparallel β strands flanked by seven α helices. The two domains are connected by a two-stranded antiparallel β sheet (the β7 strand and β15 strand), positioned like a bridge (Figure 3A). In contrast to other bacterial RNAPs, RpoBtr has an additional 12-residue β-hairpin connecting α11 and the bridge strand β15 on the β2 domain.

Overall Structure of the CarD/RNAP-β1-β2 Complex

The CarD binding site of RNAP is located at the solvent exposed surface of the β1 domain, which is approximately 70 Å away from the RNAP active site Mg^{+2} (based on the *Tth* EC; PDB ID: 2O5I) (Figure 4A). Despite the long distance between the binding site and the active site, this domain serves as an interaction module for various regulatory proteins, including sigma factors at different stages of transcription, and is important for RNAP DNA binding and open complex stability (Trinh et al., 2006; Vassylyev et al., 2002).

At the CarD-RNAP interface, the primary four-stranded β sheet of the CarD N-terminal domain forms an extended eight-stranded β sheet with the β1 domain of the RNAP β-subunit

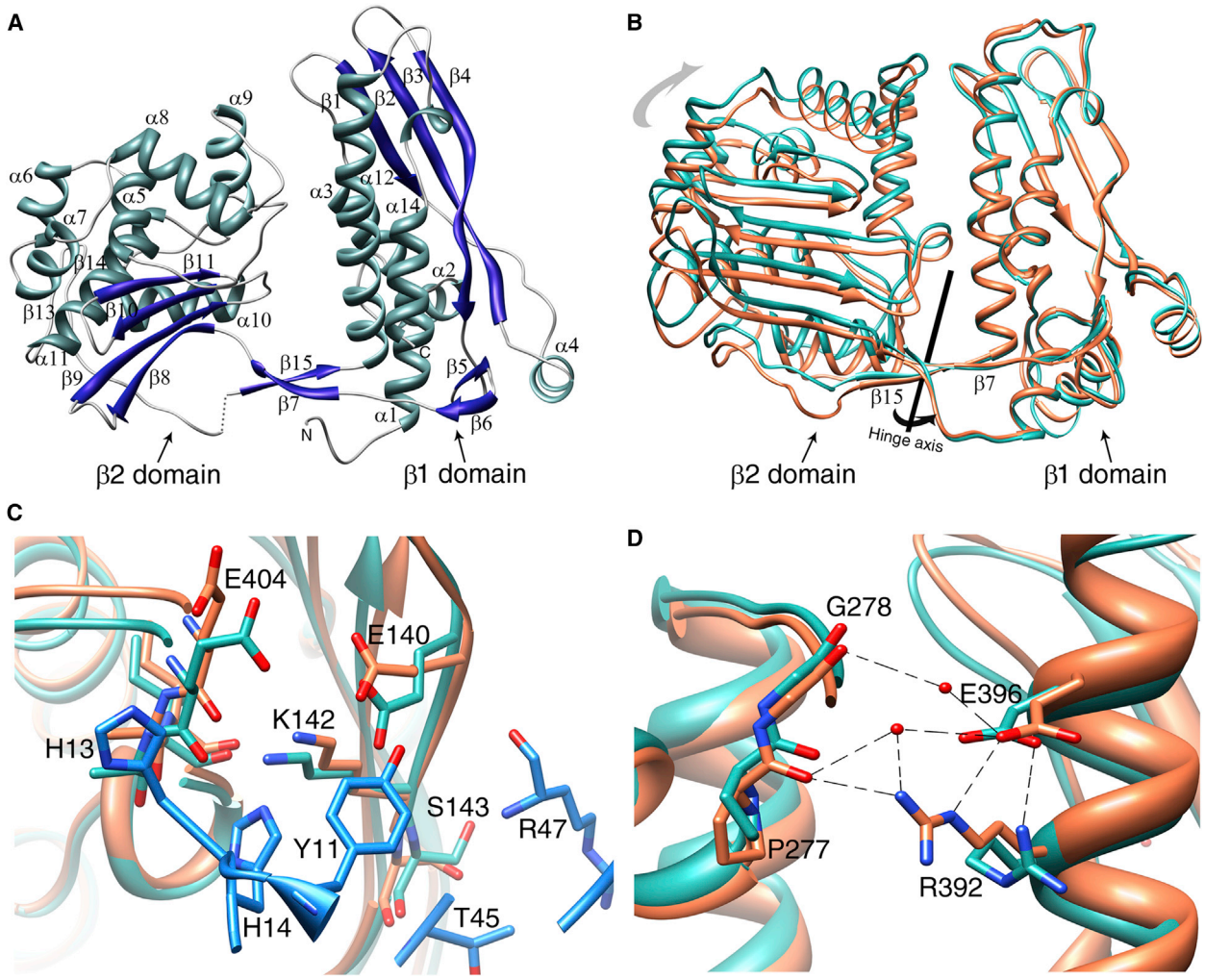

Figure 3. Conformational Differences in RpoBtr in the Uncomplexed and Complexed Forms

(A) Ribbon representation of an uncomplexed RpoBtr molecule. The secondary structure assignments were done with PDBsum server (Laskowski, 2009).

(B) The conformational differences observed in the β1-β2 domain-domain orientation between uncomplexed RpoBtr (green) and RpoBtr complexed with CarD (orange). Superposition of the β1 domains yields an rmsd of 2.8 Å over the C_αs of the β2 domains. The hinge axis centered on the two-stranded antiparallel β sheet (β7 and β15) bridging the two domains is also shown.

(C) Local conformational changes of the RNAP β1 domain residues at the CarD/RNAP interface. β1-E404, S143, and E140 change conformation to interact with CarD-H13, R47, T45, and Y11.

(D) Local conformational changes of the RNAP β1 domain residues at the β1-β2 domain interface. E396 and R392 of the β1 domain make additional water-mediated interactions with the β2 domain residues P277 and G278 in the CarD/RNAP complex. The CarD residues are shown in blue. Coloring of RpoBtr is the same as in (B). Molecular visualization and analysis, including rmsd calculations, were performed with the UCSF Chimera package (Pettersen et al., 2004). See also Figure S3.

(see Figure S2 for a stereo image). Specifically, the β4 strand of CarD comprising residues Leu44 to Pro49 forms an antiparallel β sheet with the β4 strand residues Thr138 to Gln144 of RpoBtr (1:1 heterodimer; Figures 1A and S2B). This results in a mixed β sheet in the $1_\uparrow\, 2_\downarrow\, 3_\uparrow\, 4_\downarrow\, 4'_\uparrow\, 3'_\downarrow\, 2'_\uparrow\, 1'_\downarrow$ topology. Surprisingly, association of RNAP with CarD results in only a 500 $Å^2$ (otherwise solvent exposed) buried surface area, which is below average (1,500–2,000 $Å^2$) for heteromeric protein-protein complexes (Kleanthous, 2000). While the buried surface is relatively small, it is rich in intermolecular hydrogen bonds. There are eight hydrogen bonds and 69 nonbonded contacts between RpoBtr and CarD formed by the residues located on the β4 strands of both proteins, on the loop connecting α12 and α13 of the RNAP β1 domain, and on the turn between the β1 and β2 strands of CarD. Specifically, β1-Ile141 interacts with CarD-Arg47 (2.8 Å), and β1-Ser143 interacts with CarD-Thr45 (2.7 Å) through four backbone-backbone hydrogen bonds (Figure 1B). Interestingly, the side chain-specific hydrogen bonding interactions are present only between β1-Lys142:CarD-His14 (2.9 Å), β1-Glu140:CarD-Tyr11 (2.4 Å), β1-Thr138:CarD-Asn52 (2.8 Å), and β1-Gln144:CarD-Gly42 (3.0 Å; Figure 1B). The intermolecular interface is also stabilized by electrostatic, hydrophobic, and van der Waals interactions (Figure S2). In fact, electrostatic forces contribute significantly to the CarD/RNAP interaction

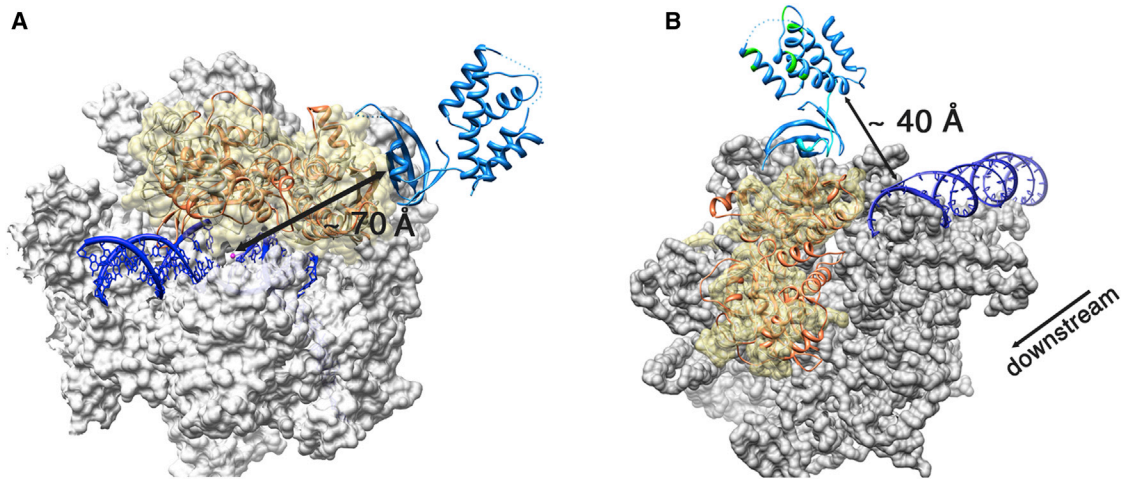

Figure 4. Superposition of the *Mtb* CarD/RNAP Complex Structure with the Bacterial Elongation and Initiation Complex Structures
The *Mtb* CarD/RNAP complex is colored as previously (RpoBtr is orange and CarD is blue).
(A) Superposition of the *Mtb* CarD/RNAP complex structure with the *Tth* RNAP EC structure (PDB ID: 2O5I). *Tth* RNAP is gray, the DNA duplex and DNA-RNA hybrid are dark blue, and the active site Mg^{+2} is shown as a magenta sphere. The molecular surface of the α and β′ subunits is shown in gray, where the β1-β2 domains of the *Tth* RNAP are represented as ribbons under a transparent yellow surface. CarD binds to the solvent exposed surface of the β1 domain, ~70 Å away from the catalytic center.
(B) Superposition of the *Mtb* CarD/RNAP complex structure with the *Taq* RNAP IC structure (PDB ID: 1L9Z). The molecular surface of the *Taq* RNAP is gray except for the β1-β2 domains, which are represented as a transparent yellow surface. The DNA duplex is colored dark blue. The flexible α1 and eight-residue loop of CarD are cyan. CarD's DNA interacting patches as determined by EMSA are green. The direction of transcription is also indicated. The CarD C-terminal DNA interaction domain lies in proximity to the downstream end of the dsDNA in the initiation complex (~40 Å).

because altering the local charge distribution at the interface was reported to abolish CarD/RNAP interaction completely (Weiss et al., 2012). A more detailed analysis of the intermolecular contacts is provided in Table 2.

In contrast to the structural model generated by homology modeling (based on *Tth* TRCF-RID/β1 structure), mutagenesis and two-hybrid assays (Weiss et al., 2012), which suggested that β1-Glu132 interacts with both Arg25 and Arg47 directly through hydrogen bonding and that these residues are critical for intermolecular interaction, we observed from the *Mtb* CarD/RNAP structure that β1-Glu132 is not in direct contact with CarD-Arg25 and CarD-Arg47 (5.0 Å and 6.1 Å, respectively). Arg25 interacts with β1-Ile141 only through van der Waals interactions and does not appear crucial for CarD/RNAP interaction. Similarly, Glu132 and Arg47 interact only through a water molecule in the CarD/RNAP crystal structure, and Arg47 is engaged in other hydrogen bonding and van der Waals interactions with β1-Ile141, β1-Glu140, and β1-Gly139 (Table 2). Therefore, loss of the CarD/RNAP interaction, as suggested by two-hybrid assays, upon E132R, R25E, and R47E mutations, should be due to these factors rather than the disruption of the direct interaction between Glu132-Arg25 and Glu132-Arg47.

Comparison of *Mtb* CarD/RNAP and *Tth* TRCF-RID/β1 complex structures reveals that CarD and TRCF-RID display a similar set of interactions with RNAP, even though there is no sequence conservation between the CarD β4- (^{43}DLTVRVP^{49}) and TRCF β4- (^{358}EGKLYLP^{364}) strands that interact with the RNAP β1 domain (except for the last proline residues; Figure S4A). CarD residues Tyr11, His13, and His14, located on the turn between β1 and β2 strands, also interact with the RNAP-β1 domain, which was not observed in the TRCF-RID/β1 structure. We have tested the contribution of Y11 and H14 to the CarD/RNAP interaction by generating CarD-Y11A-H14A mutant, and comparing the thermal stability of CarD-Y11A-H14A/RpoBtr and CarD-wt/RpoBtr complexes by ThermoFluor (DSF) experiments. The thermal denaturation profiles suggested that the CarD-Y11A-H14A/RpoBtr complex is less stable than the CarD-wt/RpoBtr complex ($Tm_{C11A–14A}$ = 37.9 ± 0.1°C versus Tm_{Cwt} = 39.2 ± 0.1°C; Figure S4B), which was also supported by the size exclusion chromatography (data not shown), consistent with our structure that these residues are involved in CarD/RNAP interaction. On the other hand, the salt bridge interaction observed in the TRCF-RID/β1 structure between residues RNAP Glu110 and TRCF Tyr362 and Arg341 (Westblade et al., 2010) is not present in CarD/RNAP structure.

DNA Binding Studies on *Mtb* CarD

Mtb CarD is classified as a CdnL protein due to the lack of a DNA-binding motif in its protein sequence. It has been proposed that CdnL proteins do not interact with DNA directly (García-Moreno et al., 2010). We have tested whether *Mtb* CarD can interact with DNA by electrophoretic mobility shift assay (EMSA).

Because CarD is required for stringent response in mycobacteria, we tested CarD binding to ribosomal protein and rRNA operons. The 200–300 base pairs (bp) upstream of the *rpsH*, 16S, 23S, and 5S rRNA genes were amplified for gel shift assays. Our results showed a clear shift of electrophoretic mobility between the free DNA and the CarD-bound DNA for these probes (Figure 5A). The gel shift assays done with various random DNA probes, as well as DNase footprinting experiments (data not shown), suggested that *Mtb* CarD does not show a sequence

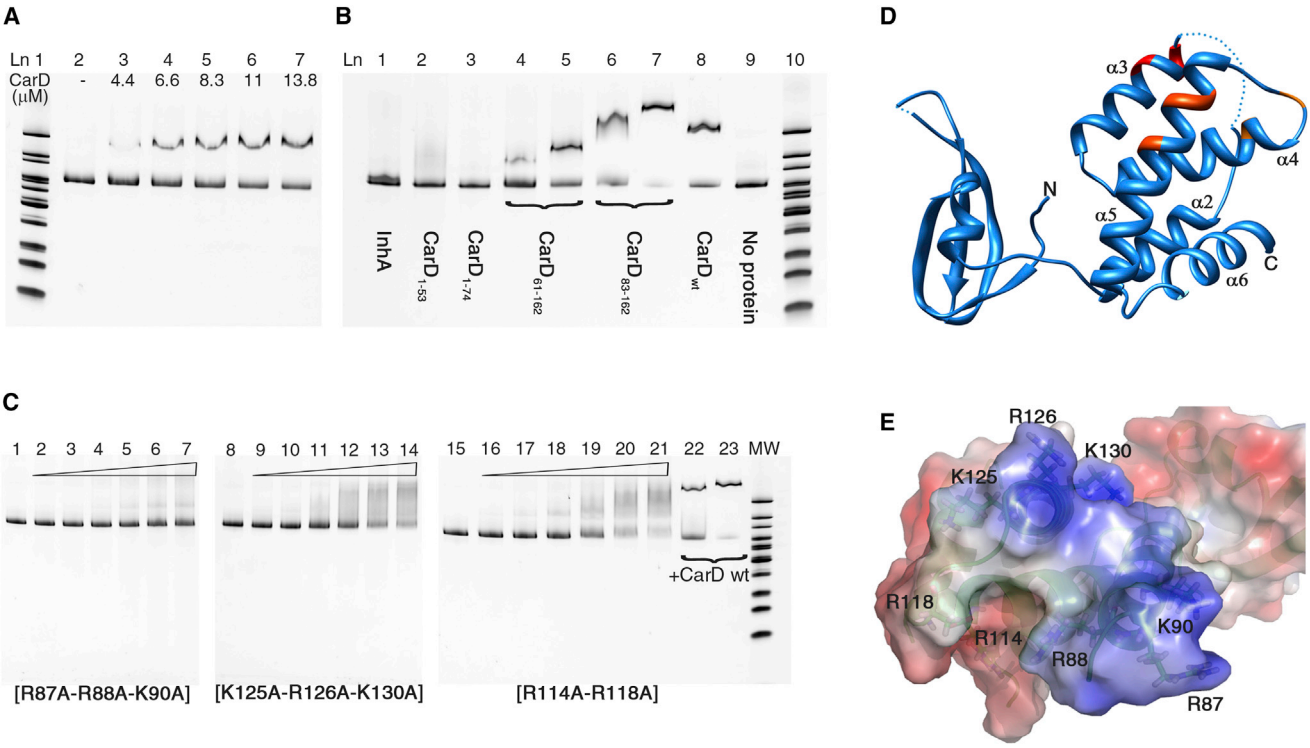

Figure 5. DNA Binding Activity of *Mtb* CarD Determined by EMSA

(A) CarD interaction with upstream DNA of 16S rRNA gene (313 bp). Lane 1: MW (molecular weight) marker. Lane 2: DNA probe, no protein. Lanes 3–7: 4.4–13.8 μM CarD.

(B) Interaction of CarD domains and a well-known non-DNA-binding protein with 16S rRNA upstream DNA probe. Lane 1: InhA (10 μM). Lane 2: $CarD_{1–53}$ (10 μM). Lane 3: $CarD_{1–74}$ (10 μM). Lanes 4 and 5: $CarD_{61–162}$ (5 and 10 μM). Lanes 6 and 7: $CarD_{83–162}$ (5 and 10 μM). Lane 8: CarD full length (10 μM). Lane 9: 16S rRNA upstream DNA probe, no protein. Lane 10: MW marker.

(C) EMSA experiments with CarD mutant proteins. Mutation of Arg and Lys residues to Ala significantly reduced the DNA-binding activity of *Mtb* CarD. R87A-R88A-K90A showed the greatest effect. Lanes 1, 8, 15: 16S rRNA upstream DNA probe, no protein. Lanes 2–7, 9–14, and 16–21: 0–44 μM mutant CarD protein (as labeled on the gel). Lanes 22 and 23: 11 and 22 μM native CarD.

(D and E) Mutations are mapped on the ribbon representation and electrostatic potential surface of CarD. R87-R88-K90 are red, K125-R126-K130 are dark orange, and R114-R118 are light orange. Gel imaging was done using the Bio-Rad Chemidoc XRS+ molecular imager, by excitation at 255 nm and emission at 520 nm. Electrostatic potential surface calculations were done with PyMol (The PyMOL Molecular Graphics System, Version 0.99rc6, Schrödinger) using APBS as the macromolecular electrostatics calculation program (Baker et al., 2001).

preference for DNA binding, indicating a nonspecific DNA-binding mode.

To elucidate the *Mtb* CarD-DNA interaction further, four different N- and C-terminally truncated CarD variants ($CarD_{61–162}$, $CarD_{83–162}$, $CarD_{1–53}$, $CarD_{1–74}$) were cloned and expressed to test each domain's DNA-binding activity. $CarD_{61–162}$ and $CarD_{83–162}$ contain the α-helical C-terminal domain and exhibited a gel shift, although with different mobilities, which could be due to the charge, size, and shape differences of the two constructs. EMSA results verified that the C-terminal domain is the DNA interaction domain (Figure 5B). The N-terminal domain is not involved in DNA interaction and is required only for RNAP interaction as observed from the CarD/RNAP structure.

Electrostatic potential surface calculations on the *Mtb* CarD structure revealed a single positively charged patch in the C-terminal domain formed by helices α3, α4, and α5 (Figures 5D and 5E). The basic residues contributing to this positively charged surface, i.e., Arg87-Arg88-Lys90 on α3, Arg114-Arg118 on α4, and Lys125-Arg126-Lys130 on α5, were mutated to alanine and subjected to EMSA. As anticipated, mutation of all the aforementioned Arg and Lys residues to Ala significantly reduced the DNA-binding activity of CarD, with the R87A-R88A-K90A mutation located on the solvent exposed surface of α3, showing the greatest effect (Figure 5C), suggesting that the CarD-DNA interaction is mainly electrostatically driven, as expected.

Sequence independent DNA-binding modes are commonly seen in bacterial nucleoid associated proteins, which are involved in chromosome compaction and structuring, DNA replication, repair, and transcription (Basu et al., 2009). The *M. xanthus* CarD protein, which has affinity for AT-rich DNA sequences, and the *M. xanthus* CdnL protein, which does not have a DNA-binding sequence motif, were both localized to the nucleoid, but this localization was proposed to occur through protein-protein interactions with RNAP (Elías-Arnanz et al., 2010; García-Moreno et al., 2010). It is plausible that *Mtb* CarD also localizes to the nucleoid in the same manner as the *M. xanthus* CdnL and *M. xanthus* CarD proteins, but considering the

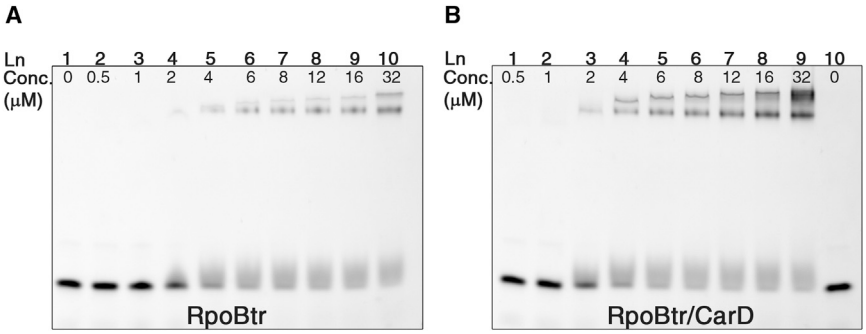

Figure 6. Comparison of the DNA Binding Activity of RpoBtr by EMSA

(A) Uncomplexed form. Lane 1: dsDNA probe, no protein. Lanes 2–10: 0.5–32 μM RpoBtr.

(B) In complex with CarD. The CarD/RpoBtr complex has higher affinity than the uncomplexed RpoBtr for the same DNA probe. Lanes 1–9: 0.5–32 μM RpoBtr/CarD complex. Lane 10: dsDNA probe, no protein.

sequence-independent DNA-binding activity, we suggest that this localization might be provided by the DNA-binding ability of CarD rather than by associating and tailing with RNAP. The C-terminal domain, and thereby the DNA-binding activity of *Mtb* CarD, is crucial for mycobacterial viability because CarD depletion cannot be complemented with the RID domain alone (Weiss et al., 2012).

Conformational Changes in RNAP upon CarD Binding

The conformation of the β1 and β2 domains observed in the CarD/RNAP complex differs from the conformations observed in the uncomplexed RpoBtr structure. Superposition of the uncomplexed RpoBtr_A and RpoBtr_B β1 domains with the CarD/RpoBtr β1 domain structure gives an rmsd of 6.8 Å and 2.8 Å, respectively, over the C_αs of the β2 domains (Figure 3B). In this context, the conformation of RpoBtr in complex with CarD is closer to the conformation of the uncomplexed RpoBtr_B molecule. It was reported in the TRCF/β1 structure that the RNAP β4 strand undergoes a "register shift" with respect to the β3 strand in the complex structure (Westblade et al., 2010). In contrast, CarD does not cause a register shift or conformational rearrangement in the β4 strand upon RNAP binding.

The CarD/RNAP β1 domain interaction causes local conformational changes primarily in the nearby RNAP side chains that are propagated through the water-mediated network of interactions and transferred to the β1-β2 domain interface and β2 domain residues. In particular, in the CarD/RNAP complex, β1-Glu404, Ser143, and Glu140 change conformation to interact with CarD-His13, Arg47, Thr45, and Tyr11, respectively (Figure 3C). The side chain of β1-Lys142 also moves 1.4 Å and loses direct H-bonding interaction with β1-Ile406, instead forming hydrogen bonds with CarD-His14 and β1-Glu140. Consecutively, the β1 domain residues Glu396 and Arg392, located at the β1-β2 domain interface of RpoBtr, adopt different conformations in CarD/RNAP complex and make additional water mediated interactions with the β2 domain residues Pro277 and Gly278 (Figure 3D). This can explain the particular conformation adopted by the two domains in the complex structure.

RNAP Regulation by CarD

The CarD/RNAP structure indicates that CarD and the functional homolog DksA regulate RNAP through different mechanisms. DksA is proposed to bind to the RNAP secondary channel, very close to the active site, to coordinate to a (p)ppGpp-bound active site Mg^{2+} ion through its coiled-coil Asp residues, and stabilize the (p)ppGpp-RNAP complex (Perederina et al., 2004). In contrast, CarD interacts with the β1 domain of the β-subunit, approximately 70 Å away from the active site, through its Tudor-fold N-terminal domain. It is interesting that even though CarD and DksA do not share sequence and structural homology, CarD can complement DksA function in a Δ*DksA E. coli* strain (Stallings et al., 2009). Furthermore, DksA is not a DNA-binding protein, whereas we have shown that CarD can interact with DNA. Whether CarD functions synergistically with (p)ppGpp the same way as DksA needs to be determined experimentally.

It is not known whether CarD regulates RNAP function during transcription initiation or elongation, or has any effect on the rate of transcription. Based on our structural data, we propose that CarD might be involved in RNAP regulation in three different ways. The first is by inducing conformational changes in the β-lobes and affecting the open complex stability and the downstream non-specific DNA-binding activity of RNAP. This can explain how *Mtb* CarD can complement DksA, which destabilizes the open complex together with (p)ppGpp during stringent response in *E. coli* (Paul et al., 2004a; Stallings et al., 2009). Bacterial RNAP β1 and β2 domains (equivalently eukaryotic RNAP II protrusion and lobe domains) are involved in various processes during transcription such as downstream DNA binding and selection of the transcription initiation site, formation and stabilization of the open complex, maintaining the proper transcription bubble via downstream DNA gripping, keeping the template and nontemplate strand-separated DNA in place during transcription initiation, and covering the DNA/RNA hybrid inside the RNAP active-site channel (Figures 4A and 4B; Lane and Darst, 2010; Murakami et al., 2002; Nechaev et al., 2000; Trautinger and Lloyd, 2002; Trinh et al., 2006). Therefore, conformational changes in this region may likely alter critical interactions of RNAP with DNA and DNA/RNA hybrid. To test if CarD interaction with the β1 domain would affect RNAP's DNA-binding affinity, we compared the nonspecific DNA-binding activity of RpoBtr in both the uncomplexed form and in complex with CarD by EMSA. Our results suggest that the CarD/RpoBtr complex has a higher affinity than the uncomplexed RpoBtr for the same DNA probe (Figure 6). We propose that CarD might affect the DNA-binding affinity of the β-lobes, and the affinity change of RpoBtr for DNA may result primarily from the conformational changes of the β-lobes induced by CarD interaction.

Overlay of the *Taq* RNAP initiation complex and CarD/RNAP complex structures show that the CarD C-terminal DNA interaction domain lies in proximity (<40 Å) to the downstream end

Table 2. Details of the Intermolecular Interactions between *Mtb* β1 Domain Residues and *Mtb* CarD

RNAP β1	CarD	Distance (Å)	Interaction Type
Thr138	Asn52	2.8	H-bond and van der Waals
	Pro49	3.5	van der Waals
	Val56	3.9	van der Waals
Gly139	Pro49	3.5	van der Waals
	Arg47	3.5	van der Waals
Glu140	Arg47	3.4	van der Waals
	Val48	3.8	van der Waals
	Tyr11	2.4	H-bond and van der Waals
	Val56	3.6	van der Waals
Ile141	Arg47	2.8	H-bond and van der Waals
	Thr45	3.4	van der Waals
	Val46	3.2	van der Waals, hydrophobic
	Arg25	3.9	van der Waals
Lys142	Thr45	3.3	van der Waals
	His14	2.9	H-bond and van der Waals
Ser143	Thr45	2.8	H-bond and van der Waals
	Leu44	3.6	van der Waals
Gln144	Leu44	3.8	van der Waals
	Asp43	3.8	van der Waals
	Gly42	3.0	H-bond and van der Waals
Glu404	His14	3.8	van der Waals
	His13	3.4	van der Waals
Ala405	His13	3.7	van der Waals
	His14	3.7	van der Waals
Thr407	His14	3.3	van der Waals

See also Figure S4.

of dsDNA in the initiation complex (Figure 4B), suggesting that CarD may interact with the promoter DNA together with RNAP during initiation. The CarD C-terminal domain is connected to the CarD N-terminal domain by a twisted α1 helix and a short loop and may adopt a different relative conformation in solution than the one observed in the crystal structure. Therefore, a second possibility is that this domain can either function as an anchor on DNA to hold CarD in place and strengthen the CarD/RNAP interaction or it can have a direct functional role in transcription regulation such as promoter selection and binding. The role of the C-terminal domain on CarD function is currently under investigation.

Another possible mechanism is allosteric regulation by inducing conformational changes around the RNAP active site despite the distance of the CarD binding site from the RNAP catalytic center. In fact, mutations at the interface that weaken the CarD/RNAP interaction were reported to make *Mtb* more susceptible to rifampicin (Rif), which binds to the RNAP active site and inhibits transcription elongation. This suggests that CarD/RNAP interaction is able to induce conformational changes not only in the β1-β2 domains but also in the Rif binding pocket, causing Rif to bind more weakly to RNAP. The clinically isolated Rif-resistant *Mtb* strains carrying mutations on distant β residues, such as Val170, which do not interact directly with Rif, affect the conformation of the Rif binding pocket, and alter the affinity of RNAP for the drug (Campbell et al., 2001). Similarly, CarD interaction with the β-lobes may result in a reduced affinity of RNAP for Rif. A more complete understanding of the effect of CarD on RNAP both structurally and functionally must await the solution of the full-length RNAP/CarD structure.

The CarD/RNAP structure presented here reveals the molecular basis of this protein-protein interaction and provides insights into RNAP regulation by CarD. EMSA experiments revealed an unexpected DNA-binding activity for *Mtb* CarD, which is required for complete in vivo function and mycobacterial viability, and is provided by a distinct domain not associated with RNAP interaction. Determination of the CarD/DNA complex and RNAP/CarD/DNA ternary complex crystal structures is needed to further characterize the transcriptional regulation by CarD.

EXPERIMENTAL PROCEDURES

Generation of Expression Constructs and Cloning

Rv3583c, encoding the *Mtb* CarD protein, and DNA encoding the *Mtb* RNAP β-subunit (*Rv0667*) residues 47–433 (labeled RpoBtr), were amplified from *Mtb* H37Rv genomic DNA by PCR. The genes were inserted into pET15b and pET30b (Novagen) expression vectors using the NdeI-BamHI and NdeI-HindIII restriction sites. The pET15b construct contained an N-terminal 6X-His tag and labeled RpoBtr-NHis, while the pET30b construct had a stop codon at the end of the gene sequence, generating an untagged protein (CarD-notag). DNA encoding the full length and truncated CarD proteins ($CarD_{1-74}$, $CarD_{1-53}$, $CarD_{61-162}$ and $CarD_{83-162}$) were amplified from *Mtb* H37Rv genomic DNA by PCR with the NdeI-HindIII restriction sites and inserted into the pET28b vector (Novagen). CarD_R87A-R88A-K90A, CarD_R114A-R118A, and CarD_K125A-R126A-K130A plasmids were generated using a site directed mutagenesis kit (Stratagene). The sequence of each construct was verified by DNA sequencing. The primers used in this study are provided in Table S1.

Expression and Purification

Expression plasmids for the uncomplexed RpoBtr, native, and mutant CarD proteins were transformed to *E. coli* BL21(DE3) cells, and recombinant protein expression was induced with 1 mM IPTG. For co-expression of *Mtb* RNAP β1-β2 domains and *Mtb* CarD, the plasmids RpoBtr-NHis and CarD-notag were cotransformed into *E. coli* Rosetta2(DE3)pLysS cells, and expression was induced with 0.75 mM IPTG. Proteins were extracted with French press and purified by metal affinity and size exclusion chromatography. The RpoBtr-NHis:CarD complex eluted as a single peak from the size exclusion column. Co-elution of RpoBtr and CarD from the IMAC and size-exclusion columns was verified by SDS-PAGE. Finally, the purified proteins were concentrated to 10 mg/ml and stored at −80°C for further use. Details of the expression and purification process are provided in the Supplemental Experimental Procedures.

Crystallization

RpoBtr-NHis-SeMet and native protein crystals were obtained using hanging-drop vapor diffusion method by incubating 2 μl of purified protein solution with 2 μl of crystallization solution (0.1 M $MgCl_2$, 0.1 M HEPES [pH 7.5], 10% [w/v] PEG4000, and 0.2 M potassium citrate tribasic monohydrate, and 20% [w/v] PEG3350, respectively) at 16°C. The RpoBtr-NHis:CarD complex was crystallized by mixing 2 μl of protein solution with 2 μl of mother liquor (2% [v/v] tacsimate [pH 5.0], 0.1 M sodium citrate tribasic dihydrate [pH 5.6], and 14% [w/v] PEG3350) by hanging-drop vapor diffusion. Crystals were cryo-protected with 20% (v/v) ethylene glycol and flash-frozen prior to data collection. Data were collected at the Advanced Light Source (ALS; Lawrence Berkeley National Laboratory) and at the Advanced Photon Source (APS beamlines 23ID and 19ID; Argonne National Laboratory) at 0.979 Å.

Data Collection and Structure Determination

The structure of the *Mtb* RNAP β-subunit β1-β2 domains was solved by single-wavelength anomalous diffraction (SAD) using RpoBtr-NHis-SeMet crystals.

Crystals belonged to the $P2_12_12_1$ space group and diffracted to 2.9 Å. Subsequently, resolution was improved to 2.5 Å by diffraction data obtained from native (non-SeMet) RpoBtr-NHis crystals. Refinement and iterative manual model building was performed with Phenix (Adams et al., 2010) and COOT (Emsley et al., 2010), and the final model had R_{work} and R_{free} values of 0.21 and 0.26, respectively.

The RpoBtr-NHis:CarD complex crystals belonged to the $C222_1$ space group and the diffraction data to 2.1 Å resolution was processed with Denzo/Scalepack. The structure was solved by MR using the RpoBtr β1 and β2 domains as two different search ensembles (Phaser, CCP4; McCoy et al., 2007; Winn et al., 2011). After locating one copy of RpoBtr in the ASU, CarD was built into the additional $|F_o|-|F_c|$ density manually. The final model included one RpoBtr:CarD complex in the ASU, and the structure was refined with Phenix Refine to a R_{work} = 0.20 and an R_{free} = 0.23. Data collection and processing statistics are provided in Table 1. Details of the data collection and structure determination are provided in the Supplemental Experimental Procedures.

EMSAs

For EMSA, DNA 200–300 bp upstream of the *rpsH*, 16S, 23S, and 5S rRNA promoters were amplified from H37Rv genomic DNA with PCR (for primers, see Table S1) and purified by gel-extraction. At room temperature, 40 ηg of double-stranded DNA was incubated with different amounts of protein (0–8 μg) for 30 min in 25 mM Tris (pH 7.5) and 50 mM NaCl. As a negative control, a known non-DNA-binding protein, enoyl-ACP reductase InhA from *Mtb*, was used to confirm that binding of *Mtb* CarD to DNA is protein-specific. The mixture was loaded on a precast 10% nondenaturing polyacrylamide gel and the gel was run at a constant voltage (120 V) with prechilled 0.5× TBE (89 mM Tris base, 89 mM boric acid, 1 mM EDTA [pH 8.0]) buffer at 4°C. After the run was completed, the gel was stained with 1× Syber green (Invitrogen) DNA stain solution for 30 min in the dark and imaged (Jing et al., 2003).

ThermoFluor Measurements

Differential scanning fluorimetry experiments were carried out with 1 μM of CarD/RpoBtr or CarD-Y11A-H14A/RpoBtr complex in 200 mM Tris (pH 7.5) 100 mM NaCl buffer, in the presence of 5× Sypro orange dye (Molecular Probes), in a 20 μl reaction volume. The temperature of the samples was changed from 25°C to 95°C at a heating rate of 0.5°C/min, and the fluorescence was monitored with an Mx3005P qPCR instrument (Agilent). The melting point (Tm) was calculated as the lowest point of the first derivative plot (DeSantis et al., 2012).

ACCESSION NUMBERS

The PDB accession numbers for coordinates of the uncomplexed RpoBtr and RpoBtr/CarD complex reported in this paper are 4KBJ and 4KBM, respectively.

SUPPLEMENTAL INFORMATION

Supplemental Information includes Supplemental Experimental Procedures, four figures, and one table and can be found with this article online at http://dx.doi.org/10.1016/j.str.2013.08.014.

ACKNOWLEDGMENTS

This work is supported by grant A-0015 from the Welch foundation (to J.C.S.) and TB Structural Genomics grant NIH P01AI095208. We would like to thank the beamline staff of APS-19 ID and APS-23-ID and Dr. Li-Wei Hung (Advanced Light Source, Lawrence Berkeley National Laboratory) for data collection and Tracey Musa and Amir Safi for careful reading of the manuscript.

Received: May 13, 2013
Revised: July 5, 2013
Accepted: August 5, 2013
Published: September 19, 2013

REFERENCES

Adams, P.D., Afonine, P.V., Bunkóczi, G., Chen, V.B., Davis, I.W., Echols, N., Headd, J.J., Hung, L.W., Kapral, G.J., Grosse-Kunstleve, R.W., et al. (2010). PHENIX: a comprehensive Python-based system for macromolecular structure solution. Acta Crystallogr. D Biol. Crystallogr. *66*, 213–221.

Baker, N.A., Sept, D., Joseph, S., Holst, M.J., and McCammon, J.A. (2001). Electrostatics of nanosystems: application to microtubules and the ribosome. Proc. Natl. Acad. Sci. USA *98*, 10037–10041.

Basu, D., Khare, G., Singh, S., Tyagi, A., Khosla, S., and Mande, S.C. (2009). A novel nucleoid-associated protein of Mycobacterium tuberculosis is a sequence homolog of GroEL. Nucleic Acids Res. *37*, 4944–4954.

Campbell, E.A., Korzheva, N., Mustaev, A., Murakami, K., Nair, S., Goldfarb, A., and Darst, S.A. (2001). Structural mechanism for rifampicin inhibition of bacterial rna polymerase. Cell *104*, 901–912.

DeSantis, K., Reed, A., Rahhal, R., and Reinking, J. (2012). Use of differential scanning fluorimetry as a high-throughput assay to identify nuclear receptor ligands. Nucl. Recept. Signal. *10*, e002.

Elías-Arnanz, M., Padmanabhan, S., and Murillo, F.J. (2010). The regulatory action of the myxobacterial CarD/CarG complex: a bacterial enhanceosome? FEMS Microbiol. Rev. *34*, 764–778.

Emsley, P., Lohkamp, B., Scott, W.G., and Cowtan, K. (2010). Features and development of Coot. Acta Crystallogr. D Biol. Crystallogr. *66*, 486–501.

Gallego-García, A., Mirassou, Y., Elías-Arnanz, M., Padmanabhan, S., and Jiménez, M.A. (2012). NMR structure note: N-terminal domain of Thermus thermophilus CdnL. J. Biomol. NMR *53*, 355–363.

García-Moreno, D., Abellón-Ruiz, J., García-Heras, F., Murillo, F.J., Padmanabhan, S., and Elías-Arnanz, M. (2010). CdnL, a member of the large CarD-like family of bacterial proteins, is vital for Myxococcus xanthus and differs functionally from the global transcriptional regulator CarD. Nucleic Acids Res. *38*, 4586–4598.

Gibrat, J.F., Madej, T., and Bryant, S.H. (1996). Surprising similarities in structure comparison. Curr. Opin. Struct. Biol. *6*, 377–385.

Gupta, R.K., Thakur, T.S., Desiraju, G.R., and Tyagi, J.S. (2009). Structure-based design of DevR inhibitor active against nonreplicating Mycobacterium tuberculosis. J. Med. Chem. *52*, 6324–6334.

Holm, L., and Rosenström, P. (2010). Dali server: conservation mapping in 3D. Nucleic Acids Res. *38*(Web Server issue), W545–W549.

Jing, D., Agnew, J., Patton, W.F., Hendrickson, J., and Beechem, J.M. (2003). A sensitive two-color electrophoretic mobility shift assay for detecting both nucleic acids and protein in gels. Proteomics *3*, 1172–1180.

Kleanthous, C. (2000). Protein-protein recognition. (Oxford, New York: Oxford University Press).

Krissinel, E., and Henrick, K. (2004). Secondary-structure matching (SSM), a new tool for fast protein structure alignment in three dimensions. Acta Crystallogr. D Biol. Crystallogr. *60*, 2256–2268.

Lane, W.J., and Darst, S.A. (2010). Molecular evolution of multisubunit RNA polymerases: sequence analysis. J. Mol. Biol. *395*, 671–685.

Laskowski, R.A. (2009). PDBsum new things. Nucleic Acids Res. *37*(Database issue), D355–D359.

McCoy, A.J., Grosse-Kunstleve, R.W., Adams, P.D., Winn, M.D., Storoni, L.C., and Read, R.J. (2007). Phaser crystallographic software. J. Appl. Cryst. *40*, 658–674.

Murakami, K.S., Masuda, S., Campbell, E.A., Muzzin, O., and Darst, S.A. (2002). Structural basis of transcription initiation: an RNA polymerase holoenzyme-DNA complex. Science *296*, 1285–1290.

Murzin, A.G., Brenner, S.E., Hubbard, T., and Chothia, C. (1995). SCOP: a structural classification of proteins database for the investigation of sequences and structures. J. Mol. Biol. *247*, 536–540.

Nechaev, S., Chlenov, M., and Severinov, K. (2000). Dissection of two hallmarks of the open promoter complex by mutation in an RNA polymerase core subunit. J. Biol. Chem. *275*, 25516–25522.

Nicolas, F.J., Cayuela, M.L., Martínez-Argudo, I.M., Ruiz-Vazquez, R.M., and Murillo, F.J. (1996). High mobility group I(Y)-like DNA-binding domains on a bacterial transcription factor. Proc. Natl. Acad. Sci. USA *93*, 6881–6885.

Paul, B.J., Barker, M.M., Ross, W., Schneider, D.A., Webb, C., Foster, J.W., and Gourse, R.L. (2004a). DksA: a critical component of the transcription initiation machinery that potentiates the regulation of rRNA promoters by ppGpp and the initiating NTP. Cell *118*, 311–322.

Paul, B.J., Ross, W., Gaal, T., and Gourse, R.L. (2004b). rRNA transcription in Escherichia coli. Annu. Rev. Genet. *38*, 749–770.

Peñalver-Mellado, M., García-Heras, F., Padmanabhan, S., García-Moreno, D., Murillo, F.J., and Elías-Arnanz, M. (2006). Recruitment of a novel zinc-bound transcriptional factor by a bacterial HMGA-type protein is required for regulating multiple processes in Myxococcus xanthus. Mol. Microbiol. *61*, 910–926.

Perederina, A., Svetlov, V., Vassylyeva, M.N., Tahirov, T.H., Yokoyama, S., Artsimovitch, I., and Vassylyev, D.G. (2004). Regulation through the secondary channel—structural framework for ppGpp-DksA synergism during transcription. Cell *118*, 297–309.

Pettersen, E.F., Goddard, T.D., Huang, C.C., Couch, G.S., Greenblatt, D.M., Meng, E.C., and Ferrin, T.E. (2004). UCSF Chimera—a visualization system for exploratory research and analysis. J. Comput. Chem. *25*, 1605–1612.

Raman, K., Yeturu, K., and Chandra, N. (2008). targetTB: a target identification pipeline for Mycobacterium tuberculosis through an interactome, reactome and genome-scale structural analysis. BMC Syst. Biol. *2*, 109.

Sacchettini, J.C., Rubin, E.J., and Freundlich, J.S. (2008). Drugs versus bugs: in pursuit of the persistent predator Mycobacterium tuberculosis. Nat. Rev. Microbiol. *6*, 41–52.

Selenko, P., Sprangers, R., Stier, G., Bühler, D., Fischer, U., and Sattler, M. (2001). SMN tudor domain structure and its interaction with the Sm proteins. Nat. Struct. Biol. *8*, 27–31.

Severinov, K., Mustaev, A., Kukarin, A., Muzzin, O., Bass, I., Darst, S.A., and Goldfarb, A. (1996). Structural modules of the large subunits of RNA polymerase. Introducing archaebacterial and chloroplast split sites in the beta and beta' subunits of Escherichia coli RNA polymerase. J. Biol. Chem. *271*, 27969–27974.

Srivatsan, A., and Wang, J.D. (2008). Control of bacterial transcription, translation and replication by (p)ppGpp. Curr. Opin. Microbiol. *11*, 100–105.

Stallings, C.L., Stephanou, N.C., Chu, L., Hochschild, A., Nickels, B.E., and Glickman, M.S. (2009). CarD is an essential regulator of rRNA transcription required for Mycobacterium tuberculosis persistence. Cell *138*, 146–159.

Tagami, S., Sekine, S., Kumarevel, T., Hino, N., Murayama, Y., Kamegamori, S., Yamamoto, M., Sakamoto, K., and Yokoyama, S. (2010). Crystal structure of bacterial RNA polymerase bound with a transcription inhibitor protein. Nature *468*, 978–982.

Trautinger, B.W., and Lloyd, R.G. (2002). Modulation of DNA repair by mutations flanking the DNA channel through RNA polymerase. EMBO J. *21*, 6944–6953.

Trinh, V., Langelier, M.F., Archambault, J., and Coulombe, B. (2006). Structural perspective on mutations affecting the function of multisubunit RNA polymerases. Microbiol. Mol. Biol. Rev. *70*, 12–36.

Vassylyev, D.G., Sekine, S., Laptenko, O., Lee, J., Vassylyeva, M.N., Borukhov, S., and Yokoyama, S. (2002). Crystal structure of a bacterial RNA polymerase holoenzyme at 2.6 A resolution. Nature *417*, 712–719.

Weiss, L.A., Harrison, P.G., Nickels, B.E., Glickman, M.S., Campbell, E.A., Darst, S.A., and Stallings, C.L. (2012). The Interaction of CarD with RNAP Mediates Mycobacterium tuberculosis Viability, Rifampicin Resistance, and Pathogenesis. J. Bacteriol.

Westblade, L.F., Campbell, E.A., Pukhrambam, C., Padovan, J.C., Nickels, B.E., Lamour, V., and Darst, S.A. (2010). Structural basis for the bacterial transcription-repair coupling factor/RNA polymerase interaction. Nucleic Acids Res. *38*, 8357–8369.

Winn, M.D., Ballard, C.C., Cowtan, K.D., Dodson, E.J., Emsley, P., Evans, P.R., Keegan, R.M., Krissinel, E.B., Leslie, A.G., McCoy, A., et al. (2011). Overview of the CCP4 suite and current developments. Acta Crystallogr. D Biol. Crystallogr. *67*, 235–242.

Zhang, Y., Feng, Y., Chatterjee, S., Tuske, S., Ho, M.X., Arnold, E., and Ebright, R.H. (2012). Structural basis of transcription initiation. Science *338*, 1076–1080.